Available online at BCREC website: https://bcrec.id

Bulletin of Chemical Reaction Engineering & Catalysis, 18 (2) 2023, 344-352

Research Article

Magnetization Study of Iron Sand from Sabang, Indonesia: The Potential of Magnetic Materials in the Photocatalytic Field

Sri Nengsih[1,2], Syahrun Nur Abdulmadjid[1,3], Mursal Mursal[3], Rinaldi Idroes[4], Zulkarnain Jalil[3,*]

[1]*Graduate School of Mathematics and Applied Science, Universitas Syiah Kuala, Banda Aceh, 23111, Indonesia.*
[2]*Department of Physics Engineering, Science and Technology Faculty, Universitas Islam Negeri Ar-Raniry Banda Aceh, 23111, Indonesia.*
[3]*Department of Physics, Natural Science and Mathematics Faculty, Universitas Syiah Kuala Banda Aceh, 23111, Indonesia.*
[4]*Department of Chemistry, Faculty of Mathematics and Natural Sciences, Universitas Syiah Kuala, Banda Aceh 23111, Indonesia.*

Received: 25th June 2023; Revised: 7th August 2023; Accepted: 8th August 2023
Available online: 10th August 2023; Published regularly: August 2023

Abstract

The magnetization of iron sand from Anoi Itam beach, Sabang, Indonesia, was investigated through sample testing and synthesis using the co-precipitation method. The purpose of this study is to analyze the magnetic properties of iron sand and review its potential in photocatalytic processes. Before being synthesized, the natural iron sand was separated and milled. The iron sand was dissolved in 37% v/v HCl, stirred, and heated for 30 min. This solution was filtered and precipitated with 6.5 M NH_4OH while stirring and heating for 30 min. The magnetite formed was washed repeatedly with distilled water until it reached a normal pH, and then dried. Magnetite characterization tests were performed using XRF, XRD, VSM, and UV-Vis spectroscopy. The test results showed that the iron sand had a high magnetic quality with a concentration of 91.17% after the synthesis process. The resulting magnetite phase structure had a spinal inverse cubic shape, with the highest peak at the Miller index (311). From the VSM test, it is known that the resulting magnetite exists in a soft magnetic form with superparamagnetic groups. From optical absorption, magnetite has a gap energy of approximately 2.8 eV. It can be concluded that the magnetite from Anoi Itam Sabang has potential as a photocatalytic absorbent in the visible light wavelength region.

Copyright © 2023 by Authors, Published by BCREC Group. This is an open access article under the CC BY-SA License (https://creativecommons.org/licenses/by-sa/4.0).

Keywords: Magnetite; co-precipitation method; iron sand; optical absorption; photocatalytic

How to Cite: S. Nengsih, S.N. Abdulmadjid, M. Mursal, R. Idroes, Z. Jalil (2023). Magnetization Study of Iron Sand from Sabang, Indonesia: The Potential of Magnetic Materials in the Photocatalytic Field. *Bulletin of Chemical Reaction Engineering & Catalysis*, 18(2), 344-352 (doi: 10.9767/bcrec.19041)

Permalink/DOI: https://doi.org/10.9767/bcrec.19041

1. Introduction

The study of iron sand has attracted the interest of scientists both in the fields of science and engineering. Various types of research have been carried out in improving the quality of iron sand. One of them is by making iron sand in nanometer size. Through various preparation techniques, it has been informed through journals about iron sand processing, both local scale jour-

* Corresponding Author.
Email: zjalil@unsyiah.ac.id (Z. Jalil)

nals and international scale journals. There is research on the synthesis of Fe_2O_3 from iron sand using the hydrochloric acid dissolved metal method [1], synthesis of iron sand on the study of crystal structure and dielectricity of nanoparticles magnetite based on Zn^{2+} iron sand doped synthesized by the co-precipitation method [2], synthesis and magnetic properties of Fe_3O_4-Montmorillonite nanocomposites based on temperature variations [3]. Other studies also discuss magnetic iron oxide nanoparticles: synthesis and surface coating techniques for biomedical applications [4], synthesis of Fe_3O_4 nanoparticles and their magnetic properties [5] and synthesis and characteristics of black, red and yellow nanoparticles from iron sand [6].

The existence of iron sand in Aceh Province has been studied to predict the content of mineral compounds. Several studies have shown that iron sand has the potential to be used in producing magnetite nanoparticles [1,7–13]. Preparation of nanoparticles that have been developed in Fe_3O_4 powder has been carried out using the co-precipitation method [14–18], spray pyrolysis method, forced hydrolysis method, iron hydroxide reduction oxidation reaction method, iron hydroxide microwave irradiation, iron(III) nitrate combustion, micro emulsion techniques and hydrothermal preparation techniques [16]. Apart from the co-precipitation method, all of these methods cannot be used on a large scale due to low synthesis results, clumping formation and non-uniform size distribution.

The co-precipitation synthesis method is the method chosen in this study because the synthesis is the most commonly used to produce magnetic nanoparticles. This co-precipitation synthesis method is an easy method to produce large quantities of magnetic particles [19]. No special stabilizing agent is required during the synthesis process and the product can be dissolved in water which is promising for environmentally friendly applications [15].

From several studies, magnetite (Fe_3O_4) has been used to form composites with TiO_2 particles due to its high magnetic properties, low toxicity and biocompatible in living tissues [20–26]. In addition, Fe_3O_4 nanoparticles have a small energy band <3 eV so they can be used in the photocatalyst process. Another advantage of Fe_3O_4 nanoparticles with the addition of TiO_2 particles is that they can slow down the formation of recombination between holes and electrons in Fe_3O_4 nanoparticles in the photocatalytic process [27,28].

The ability of TiO_2 photocatalysts in the Ultraviolet region (λ < 400 nm) is very good but the ability to absorb it is low in visible light [29]. This causes the mass transfer of TiO_2 to be limited in the photocatalytic degradation process, thereby reducing the effectiveness of TiO_2 in water treatment. As a result, the affinity for organic pollutants is weak; their absorption is low, resulting in a slow photocatalytic degradation rate. In addition, there are also challenges in the process of recovering TiO_2 particles from water treatment both from the economic and safety fields [30]. Several studies by forming TiO_2 composite nanoparticles with magnetic [31–33]. The results obtained from the magnetic-TiO_2 photocatalyst present an increase in separation properties when an external magnetic field is used [34]. This makes the photocatalyst material recoverable due to its magnetic properties such as superparamagnetism [35–37].

Therefore, the study of the magnetic properties of iron sand from Sabang needs to be investigated as a material that plays an important role in the photocatalytic process. Another cause, namely the abundance of magnetite in iron sand, has not been supported by efforts to optimize this material, so this study is important in improving the functional quality of this iron sand.

2. Materials and Methods

2.1 Materials and Tools

Iron sand was collected from Anoi Itam Beach in Sabang, Aceh Province, Indonesia. HCl (37% v/v) from Merck, NH4OH from Merck, and Aquades produced from Merck Millipore Ultrapure (Type 1) water. The equipment used was a 100 mesh sieve, scales, bar magnets, ball mill with a Planetary Mill (Fritsch, P6), Erlenmeyer, magnetic stirrer, filter paper, pH meter, mortar, and oven.

2.2 Magnetite Nanoparticle Synthesis

The co-precipitation method is used in the synthesis of magnetite nanoparticles because the simple synthesis process does not require high temperatures or lower research costs. Here are the stages: In the first stage, Iron Sand is first washed thoroughly with distilled water and then dried. The iron sand was then separated from the non-magnetic material using a bar magnet with five repetitions and sieved. In the next process, the iron sand was ground with a Ball Mill with a ball-to-sand ratio of 5:1 with a rotating speed of 350 rpm (rotations per minute) for 5 h.

Copyright © 2023, ISSN 1978-2993

In the second stage, 20 g of milled iron sand was weighed, mixed with 50 ml of HCl in an Erlenmeyer flask, stirred with a magnetite stirrer at a rotational speed of 800 rpm, and heated at 80 °C for 30 min. After the iron sand was dissolved, it was filtered through a filter paper. The filtered solution was then mixed with 6.5 M NH_4OH at a ratio of 1:5. This solution was stirred using a magnetite stirrer at a rotational speed of 800 rpm and heated at 80 °C for 30 min. The same was also done for other variations of magnetite, which was rotated at 900 rpm and 1000 rpm. This precipitate formed magnetite, which was then washed several times with distilled water and once with ethanol. The acidity of the solution was measured using a pH meter if it reached a normal pH of 7. When the normal pH was reached, the magnetite was filtered and dried in an oven at 100 °C for 1 h. The dried sample was dark black and hardened, and then the magnetite sample was ground using a mortar and pestle.

2.3 Characterization of Magnetite Nanoparticles

The chemical compounds on the iron sand and magnetite were measured using XRF Panalytical type Minipal 4, and the phase structure was investigated using XRD (Shimadzu MAXima). Furthermore, the optical absorption of magnetite was determined using by Vis spectrophotometer (Shimadzu UV-1280). Finally, the magnetic properties of iron sand and magnetite were observed using a Vibrating Sample Magnetometer (Oxford YSMI.2H). For the VSM test, the samples were cut to a size of 2x2x2 mm and then weighed less than 10 mg, as the optimum function of the sensor system on the VSM. The sample was then placed in a small container and inserted into the sample holder rod. For hysteresis measurements (M versus H), the measured data are the magnetization data as a function of a given external magnetic field.

3. Results and Discussion

The magnetite properties of iron sand from Anoi Itam, Sabang were successfully synthesized by the co-precipitation method. The elemental and compound contents of the iron sand were identified using XRF, and the test results are shown in Table 1.

Table 1 shows that the dominant elements are Fe and Ti, along with their compounds Fe_2O_3 and TiO_2. An increase in the total concentration of Fe from each treatment (PBA, 86.22%; PBM, 90.44%; and PBI, 91.17%. However, it is different from the total concentration of Ti, which decreased from 6.08% to 4.31% after the synthesis process. However, the concentrations of Si, Al, and Br were lost after the synthesis process. Likewise, the concentrations of other elements decreased after processing by separation, grinding, and synthesis. The crys-

Table 1. Percentage of concentrations of elements and compounds in Anoi Itam Sabang iron sand.

Element	Total concentration (%)			Compound	Total concentration (%)		
	PBA	PBM	PBI		PBA	PBM	PBI
Al	2	0	0	Al_2O_3	3	0	0
Si	1.6	0	0	SiO_2	2.7	0	0
P	0.31	0.26	0.25	P_2O_5	0.54	0.46	0.46
Ca	0.52	0.42	0.36	CaO	0.54	0.45	0.38
Ti	6.08	5.22	4.37	TiO_2	7.43	6.49	5.46
V	0.44	0.42	0.44	V_2O_5	0.57	0.56	0.58
Cr	0.11	0.23	0.2	Cr_2O_3	0.11	0.25	0.22
Mn	0.53	0.47	0.47	MnO	0.48	0.43	0.44
Fe	86.22	90.44	91.17	Fe_2O_3	83.15	89.37	90.37
Zn	0.09	0.08	0.09	ZnO	0.07	0.07	0.08
Br	0.33	0	0.37	Br	0.22	0	0.25
Rb	0	0.49	0.45	Rb_2O	0	0.36	0.33
Eu	0.79	0.86	0.87	Eu_2O_3	0.63	0.71	0.71
Re	0.3	0.3	0.2	ReO_7	0.2	0.3	0.2
Bi	0.83	0.8	0.75	Bi_2O_3	0.6	0.6	0.56

Note:
PBA: Natural iron sand
PBM : Iron Sand sieved + separated + milled
PBI : Iron Sand sieved + separated + milled + synthesized by co-precipitation method.

Copyright © 2023, ISSN 1978-2993

tal structures of the iron sand and magnetite were examined using XRD, as shown in Figure 1.

Based on Figure 1, natural iron sand and magnetite have the same crystal structure, namely spinal inverse cubic with reference data JCPDS 00-019-0629. Based on the reference data, four peaks appeared for iron sand and five peaks appeared for magnetite. There was a significant change in the sharpness of the resulting peaks; when it was still in the form of natural iron sand, the highest and sharpest peaks were observed at the Miller index (511), whereas after the synthesis process from iron sand into magnetite, the highest and sharpest peaks were observed at the Miller index (311). However, several other peaks were present in this chart. Based on the XRF results of identifying the presence of elements and compounds, it was found that the peak positions matched for Vanadium Pentoxide (V_2O_5) and manganese oxide (MnO) compounds. The presence of the Vanadium Pentoxide peak remained even though the iron sand was treated and processed into magnetite, whereas the wide manganese oxide peak at the beginning of the process became undetectable when the stirring speed was increased.

The crystal size can be calculated using the Scherer equation, and it was found that the range of crystal size values in iron sand varies greatly, from 16.24 to 80.33 nm. In magnetite form, the crystal size was found to be more uniform, from 10.77 to 16.23 nm. The calculation of the average value of the crystal size with error is shown in Table 2.

Based on Table 2, it can be seen that the crystal sizes of natural iron sand, milled iron sand, and magnetite with variations in stirring speed are below 100 nm. Under the condition that is still in the form of natural iron sand, the crystal size is very diverse, as indicated by the high error value obtained. When iron sand is separated from non-magnetic materials and added to the grinding process, the crystal size decreases, and the error is not too high. After synthesizing iron sand into magnetite using the co-precipitation method, the crystal size became more uniform and smaller, as indicated

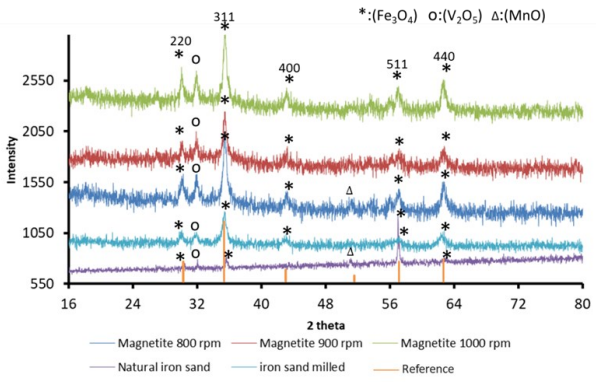

Figure 1. XRD pattern of iron sand and magnetite from Anoi Itam, Sabang.

Table 2. The average crystal size of iron sand and magnetite from Anoi Itam Sabang.

No	Sample	Average crystal size (nm)
1	Natural iron sand	80.33 ± 36.76
2	Iron sand sieved	16.24 ± 14.7
3	Fe_3O_4 800 rpm	13.97 ± 1.17
4	Fe_3O_4 900 rpm	11.98 ± 1.35
5	Fe_3O_4 1000 rpm	14.03 ± 1.88

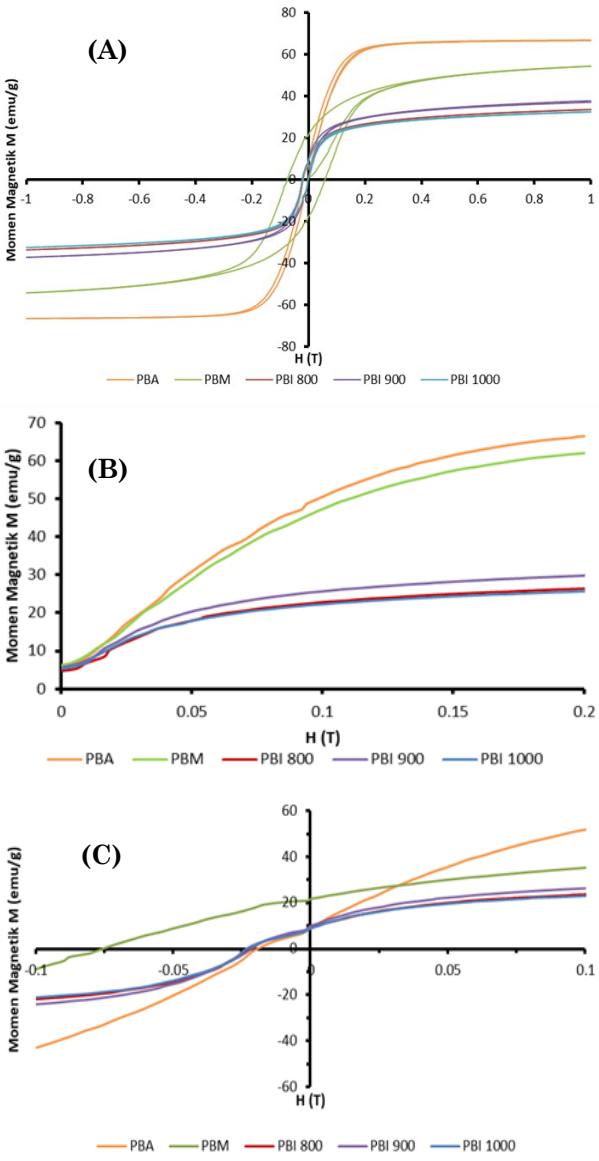

Figure 2. M-H hysteresis curve of iron sand and magnetite from Anoi Itam, Sabang.

Copyright © 2023, ISSN 1978-2993

by the low error value obtained at stirring speeds of 800, 900, and 1000 rpm. The magnetic properties of iron sand and magnetite were also studied using VSM, and the results are shown in Figure 2, where PBA is natural iron sand, PBM is separated and milled iron sand, and PBI is iron sand synthesized by the co-precipitation method at stirring speeds of 800, 900, and 1000 rpm.

Based on the M-H relationship in Figure 2(A), the hysteresis pattern of iron sand and magnetite can be observed, where M is the magnetic moment and H is the magnetic field. There are 3 things that can be observed from the shape of the M-H curve: saturation magnetization (Ms), remanent magnetization (Br), and coercivity field (Hc). The saturation magnetization (Ms) can be obtained from the saturation value achieved by magnetization from a given increase in the value of the magnetic moment (M). This indicates that the magnetic spins in the material are unidirectional. Based on Figure 2(B), it is known that natural iron sand and milled iron sand have higher Ms Values than the synthesized iron sand. As shown in Table 3, the highest Ms value was obtained at 66.626 emu/g from natural iron sand, and the lowest from iron sand synthesized at a stirring speed of 1000 rpm was 32.4254 emu/g. The remanent magnetization (Br) can be determined from the residual magnetization value when the magnetic moment (M) is removed or is zero (0). From Figure 2(C) and Table 3, it can be seen that the highest residual magnetization value is in milled iron sand, and the lowest is in iron sand synthesized at 1000 rpm. While the value of the coercivity (Hc) field is obtained from the value of the magnetic field (H) which is zero or

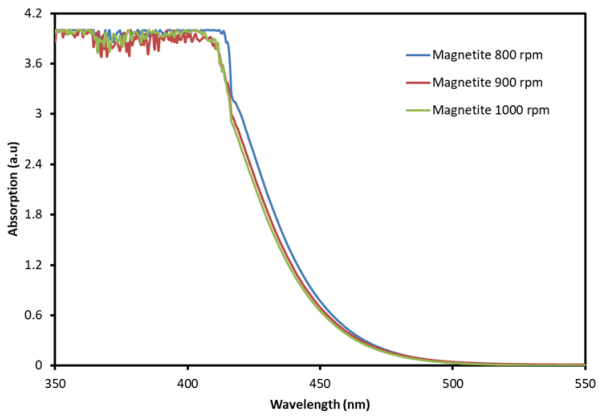

Figure 3. Optical absorption of 0.1% w/v magnetite in 3 M HCl solution for variations in solution stirring speed 800, 900 and 1000 rpm.

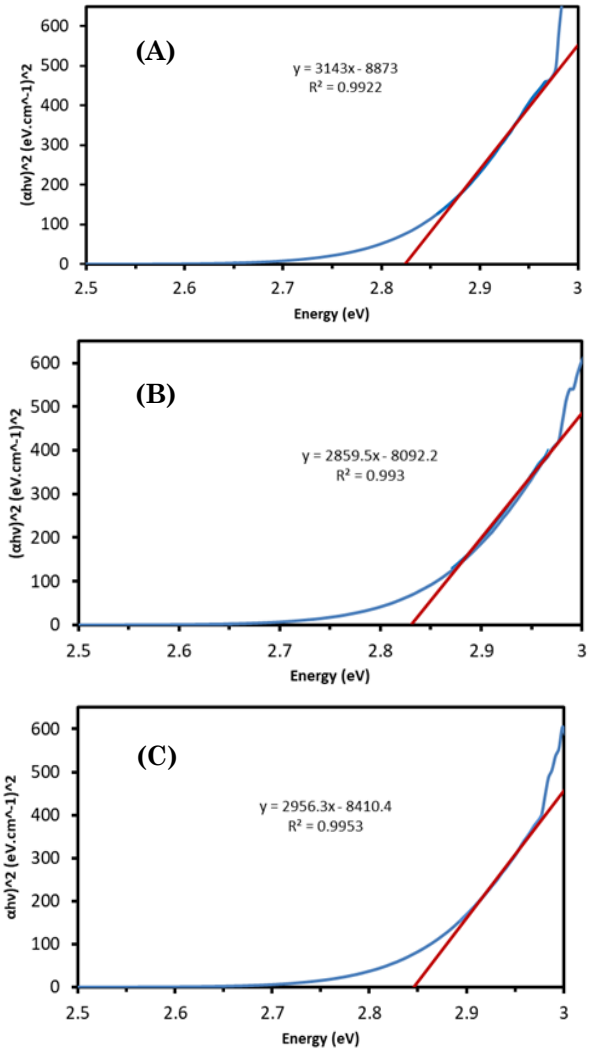

Figure 4. Gap energy of magnetite using Touc Plot method for variation of stirring speed (A) 800 rpm, (B) 900 rpm, (C) 1000 rpm.

Table 3. Magnetic properties of iron sand and magnetite from Anoi Itam, Sabang.

Sample	Ms (emu/g)	Br (emu/g)	Hc (T)
PBA	66.626	9.826	0.0205
PBM	54.3669	21.7173	0.0767
PBI800	33.5143	9.2283	0.0251
PBI900	37.7407	9.7531	0.0218
PBI1000	32.4254	8.86	0.0234

Copyright © 2023, ISSN 1978-2993

the field to remove Br. Based on Figure 2(C) and Table 3 it can be seen that the highest Hc value is in milled iron sand and the lowest Hc value is in natural iron sand. The low Hc value indicates that the resulting iron sand and magnetite are soft magnetic type. Based on the obtained VSM data, there are differences in the magnetic values of the materials for variations in stirring speed of 800, 900 and 1000 rpm for Ms, Br and Hc values. This is related to the size of the magnetite crystals formed and can be explained by the theory of magnetic domains [18]. In addition, optical absorption testing of magnetite was also carried out using a UV-Vis spectrophotometer. The test results are shown in Figure 3. This test was carried out on variations of magnetite which were given a stirring speed of 800 rpm, 900 rpm, and 1000 rpm. From Figure 3 it is shown that optical absorption in magnetite occurs from a wavelength of 400–500 nm. A change in the optical absorption value in that wavelength range indicates that there is a transition of electrons in the energy gap.

Analysis for the gap energy value of this magnetite is shown in Figure 4. In Figure 4, there are 3 graphs of the band gap energy of 0.1% b/v magnetite in 3 M HCl for variations in stirring speed using the Touc Plot method and the regression equation and its determination value are included. With the extrapolation used, we get a magnetic gap energy value of around 2.8 eV. From the regression equation, it has a determination value of R^2 close to 1 which is categorized as strong.

In determining the magnitude of the band gap energy, based on the regression equation, the values shown in Table 4 can be obtained. In Table 4, the analysis of the Touc Plot method with the indirect band gap formula is used for electron transition values. The band gap energy value indicates the location of the sudden change in absorbance between the ultraviolet and visible regions. This change in optical absorption value indicates a transition of electrons from the valence band to the conduction band. The magnitude of this band gap energy is related to the wavelength of the photon. That is, the amount of light energy imparted to the material at a certain wavelength, the energy gap is equivalent to the width of the gap in the material.

From the testing of iron sand and magnetite, it was obtained that the concentration of Fe increased after the synthesis process. The same result was shown by Rahmawati *et al.* [12], which after the synthesis process with co-precipitation and sonication methods there was an increase in the concentration of Fe. The presence of non-magnetic material also decreases the level of concentration. From the process of separation and grinding of the iron Anoi Itam sand of Sabang, it showed better crystalline properties and was followed by the synthesis process. This is in accordance with the study of Jalil *et al.* [7], which obtained fine sand from iron sand. The existence of a gap energy value in Magnetite is in the value of 2.8 eV which can be optimized in the photocatalytic process at the wavelength of visible light when it is composited with TiO_2 as the photocatalyst.

There have been several photocatalytic studies of Fe_3O_4@TiO_2 materials in the form of core-shells and Polyvinyl Pyrrolidone (PVP) as nanocatalysts in the degradation of Congo red textile dyes which have been successfully carried out. The results showed that the contribution of the addition of Fe_3O_4 concentration could be observed in changes in sample grain size. The higher concentration of Fe_3O_4 can increase the percentage of Congo red dye degradation [38].

4. Conclusion

The magnetite properties study of iron sand from Anoi Itam, Sabang were successfully synthesized by the co-precipitation method. The synthesis process has been chosen for variations of the magnetite stirring speed of 800 rpm, 900 rpm and 1000 rpm. Tests on iron sand and magnetite have been carried out using XRF, XRD, VSM and UV-Vis spectrophotometers. The increase in magnetic yield was found after the preparation of natural iron sand and the synthesis process using the co-precipitation method. Magnetite crystal size is also in the range of 11-14 nm and the maxi-

Table 4. Band gap energy of magnetite 0.1% w/v in 3 M HCl 37 % v/v.

No.	Variation of stirring speed magnetite (rpm)	Regression equation	Band gap energy (eV)
1	Magnetite 800 rpm	Y = 3143 X – 8873	2.823099
2	Magnetite 900 rpm	Y = 2859.5 X – 8092.2	2.829935
3	Magnetite 1000 rpm	Y = 2956.3 X – 8410.4	2.844907

Copyright © 2023, ISSN 1978-2993

mum Miller index is at the (311) peak. Magnetic studies from the VSM test show that the resulting magnetite is categorized as soft magnetic in the superparamagnetic group. Meanwhile, from the optical absorption value, this magnetite has the potential to be used in the photocatalytic field.

Acknowledgment

The authors acknowledge the Directorate of Research, Technology, and Community Service, Ministry of Education, Culture, Research and Technology, Republic of Indonesia for their sponsorship under PDD-doctoral dissertation research scheme, contract number: 675/UN11.2.1/PT.01.03/DRPM/2023.

CRediT Author Statement

Author Contributions: **S. Nengsih**: Conceptualization, Methodology, Investigation, Resources, Formal Analysis, Data Curation, Writting Draft Preparation, visualization; **S.N. Abdulmadjid**: Validation, Writing-Review and Editing, Data Curation, Supervision, Project Administration; **M. Mursal**: Validation, Writing-Review and Editing, Data Curation, Supervision, Project Administration, **R. Idroes**: Conceptualization; **Z. Jalil**: Conceptualization, Methodology, Investigation, Resources, Data Curation, Writing-Review and Editing, Supervision, Project Administration.

References

[1] Kartika, D.L., Pratapa, S. (2014). Sintesis Fe_2O_3 dari Pasir Besi dengan Metode Logam terlarut asam klorida. *Jurnal Sains dan Seni ITS*, 3(2), B33–B35.

[2] Taufiq, A., Bahtiar, S., Hidayat, N., Fuad, A., Diantoro, M., Hidayat, A., Pratapa, S., Darminto, D. (2012). Kajian Struktur Kristal Dan Dielektrisitas Nanopartikel Magnetite Berbasis Pasir Besi Doping Zn^{2+} Hasil Sintesis Metode Kopresipitasi. *Jurnal Sains Materi Indonesia*, 13(2), 153–156.

[3] Simamora, P., Krisna, K. (2015). Sintesis Dan Karakterisasi Sifat Magnetik Nanokomposit Fe_3O_4–Montmorilonit Berdasarkan Variasi Suhu. *Prosiding Seminar Nasional Fisika UNJ*, IV, 75–80. Retrieved from https://journal.unj.ac.id/unj/index.php/prosidingsnf/article/view/5181

[4] Ganapathe, L.S., Mohamed, M.A., Yunus, R.M., Berhanuddin, D.D. (2020). Magnetite (Fe_3O_4) nanoparticles in biomedical application: From synthesis to surface functionalisation. *Magnetochemistry*, 6(4), 1–35. DOI: 10.3390/magnetochemistry6040068.

[5] Morel, M., Martínez, F., Mosquera, E. (2013). Synthesis and characterization of magnetite nanoparticles from mineral magnetite. *Journal of Magnetism and Magnetic Materials*, 343, 76–81. DOI: 10.1016/j.jmmm.2013.04.075.

[6] Mufti, N., Atma, T., Fuad, A., Sutadji, E. (2018). Synthesis and Characterization of Black, Red and Yellow Nanoparticles Pigments from the Iron Sand. *AIP Conference Proceeding*, 1617, 165–169. DOI: 10.1063/1.4897129.

[7] Jalil, Z., Rahwanto, A., Mulana, F., and Handoko, E. (2019). Synthesis of nanohematite (Fe_2O_3) extracted from natural iron ore prepared by mechanical alloying method. *AIP Conference Proceedings*, 2151, 020041, DOI: 10.1063/1.5124671.

[8] Jalil, Z., Sari, E.N., AB, I., Handoko, E. (2014). Studi Komposisi Fasa dan Sifat Kemagnetan Pasir Besi Pesisir Pantai Aceh yang Dipreparasi dengan Metode Mechanical Milling. *Indonesian Journal of Applied Physics*, 04(1), 110–114.

[9] Nengsih, S. (2019). Karakteristik Nanopartikel Magnetite Besi Oksida Lampanah Aceh Besar Melalui Metode Kopresipitasi. *Elkawnie*, 5(1), 76. DOI: 10.22373/ekw.v5i1.4517.

[10] Bukit, N., Frida, E., Sinaga, P.S.T. (2015). Analisis Difraksi Nanopartikel Fe_3O_4 Metode Kopresipitasi Dengan Polietilen Glikol 6000. *Prosiding Seminar Nasional Fisika*, 4(7), 163–166.

[11] Hayati, R., Astuti, A. (2015). Sintesis Nanopartikel Silika Dari Pasir Pantai Purus Padang Sumatera Barat Dengan Metode Kopresipitas. *Jurnal Fisika Unand*, 4(3), 282–287.

[12] Rahmawati, R., Permana, M.G., Harison, B., Nugraha, N., Yuliarto, B., Suyatman, S., Kurniadi, D. (2017). Optimization of Frequency and Stirring Rate for Synthesis of Magnetite (Fe_3O_4) Nanoparticles by Using Coprecipitation- Ultrasonic Irradiation Methods. *Procedia Engineering*, 170, 55–59. DOI: 10.1016/j.proeng.2017.03.010.

[13] Susilawati, S., Doyan, A., Taufik, M., Wahyudi, W., Gunawan, E.R., Kosim, K., Fitriani, A., Khair, H. (2018). Identifikasi Kandungan Fe pada Pasir Besi Alam di Kota Mataram. *Jurnal Pendidikan Fisika dan Teknologi*, 4(1), 105–110. DOI: 10.29303/jpft.v4i1.571.

[14] Mascolo, M.C., Pei, Y., Ring, T.A. (2013). Room Temperature Co-Precipitation Synthesis of Magnetite Nanoparticles in a Large ph Window with Different Bases. *Materials*, 6(12), 5549–5567. DOI: 10.3390/ma6125549.

Copyright © 2023, ISSN 1978-2993

[15] Cheng, Z., Tan, A.L.K., Tao, Y., Shan, D., Ting, K.E., Yin, X.J. (2012). Synthesis and characterization of iron oxide nanoparticles and applications in the removal of heavy metals from industrial wastewater. *International Journal of Photoenergy*, 2012 DOI: 10.1155/2012/608298.

[16] Awwad, A.M., Salem, N.M. (2013). A Green and Facile Approach for Synthesis of Magnetite Nanoparticles. *Nanoscience and Nanotechnology*, 2(6), 208–213. DOI: 10.5923/j.nn.20120206.09.

[17] Nkurikiyimfura, I., Wang, Y., Safari, B., Nshingabigwi, E. (2020). Temperature-dependent magnetic properties of magnetite nanoparticles synthesized via coprecipitation method. *Journal of Alloys and Compounds*, 846, 156344. DOI: 10.1016/j.jallcom.2020.156344.

[18] Sunaryono, S., Taufiq, A., Mashuri, M., Pratapa, S., Zainuri, M., Triwikantoro, T., Darminto, D. (2015). Various magnetic properties of magnetite nanoparticles synthesized from iron-sands by coprecipitation method at room temperature. *Materials Science Forum*, 827, 229–234. DOI: 10.4028/www.scientific.net/MSF.827.229.

[19] Laurent, S., Forge, D., Port, M., Roch, A., Robic, C., Vander Elst, L., Muller, R.N. (2008). Magnetic iron oxide nanoparticles: Synthesis, stabilization, vectorization, physicochemical characterizations and biological applications. *Chemical Reviews*, 108(6), 2064–2110. DOI: 10.1021/cr068445e.

[20] Ali, A., Zafar, H., Zia, M., ul Haq, I., Phull, A.R., Ali, J.S., Hussain, A. (2016). Synthesis, characterization, applications, and challenges of iron oxide nanoparticles. *Nanotechnology, Science and Applications*, 9, 49–67. DOI: 10.2147/NSA.S99986.

[21] Aragaw, T.A., Bogale, F.M., Aragaw, B.A. (2021). Iron-based nanoparticles in wastewater treatment: A review on synthesis methods, applications, and removal mechanisms. *Journal of Saudi Chemical Society*, 25(8), 101280. DOI: 10.1016/j.jscs.2021.101280.

[22] Fernandes, Í.L., Barbosa, D.P., de Oliveira, S.B., da Silva, V.A., Sousa, M.H., Montero-Muñoz, M., Coaquira, J.A.H. (2022). Synthesis and characterization of the MNP@SiO2@TiO_2 nanocomposite showing strong photocatalytic activity against methylene blue dye. *Applied Surface Science*, 580, 152195. DOI: 10.1016/j.apsusc.2021.152195.

[23] Mufti, N., Munfarriha, U., Fuad, A., Diantoro, M. (2016). Synthesis and photocatalytic properties of Fe_3O_4@TiO_2 core-shell for degradation of Rhodamine B. *AIP Conference Proceedings*, 1712, 050009. DOI: 10.1063/1.4941892.

[24] Rani, N., Dehiya, B.S. (2020). Influence of anionic and non-ionic surfactants on the synthesis of core-shell Fe_3O_4@TiO_2 nanocomposite synthesized by hydrothermal method. *Ceramics International*, 46(15), 23516–23525. DOI: 10.1016/j.ceramint.2020.06.122.

[25] Gupta, A.K., Gupta, M. (2005). Synthesis and modification of iron oxide nanoparticles (magnetite) for biomedical applications. *Biomaterials*, 26(9), 3995–4021. DOI: 10.1016/j.biomaterials.2004.10.012.

[26] Shen, L., Qiao, Y., Guo, Y., Meng, S., Yang, G., Wu, M., Zhao, J. (2014). Facile co-precipitation synthesis of shape-controlled magnetite nanoparticles. *Ceramics International*, 40, 1519–1524. DOI: 10.1016/j.ceramint.2013.07.037.

[27] Bisaria, K., Sinha, S., Singh, R., Iqbal, H.M.N. (2021). Recent advances in structural modifications of photo-catalysts for organic pollutants degradation – A comprehensive review. *Chemosphere*, 284, 131263. DOI: 10.1016/j.chemosphere.2021.131263.

[28] Harifi, T., Montazer, M. (2014). A novel magnetic reusable nanocomposite with enhanced photocatalytic activities for dye degradation. *Separation and Purification Technology*, 134, 210–219. DOI: 10.1016/j.seppur.2014.06.042.

[29] Dong, H., Zeng, G., Tang, L., Fan, C., Zhang, C., He, X., He, Y. (2015). An overview on limitations of TiO_2-based particles for photocatalytic degradation of organic pollutants and the corresponding countermeasures. *Water Research*, 79, 128–146. DOI: 10.1016/j.watres.2015.04.038.

[30] Amir, M.N.I., Julkapli, N.M., Bagheri, S., Yousefi, A.T. (2015). TiO_2 hybrid photocatalytic systems: Impact of adsorption and photocatalytic performance. *Reviews in Inorganic Chemistry*, 35(3), 151–178. DOI: 10.1515/revic-2015-0005.

[31] Muhammad, M., Fatmaliana, A., Jalil, Z. (2019). Study of hematite mineral (Fe_2O_3) extracted from natural iron ore prepared by co-precipitation method, *IOP Conf. Series: Earth and Environmental Science*, 348 (012135), DOI: 10.1088/1755-1315/348/1/012135

[32] Govindhan, P., Pragathiswaran, C., Chinnadurai, M. (2018). A magnetic Fe_3O_4 decorated TiO_2 nanoparticles application for photocatalytic degradation of methylene blue (MB) under direct sunlight irradiation. *Journal of Materials Science: Materials in Electronics*, 29(8), 6458–6469. DOI: 10.1007/s10854-018-8627-x.

Copyright © 2023, ISSN 1978-2993

[33] Dubey, M., Kumar, R., Srivastava, S.K., Joshi, M. (2021). Visible light induced photodegradation of chlorinated organic pollutants using highly efficient magnetic Fe_3O_4/TiO_2 nanocomposite. *Optik*, 243, 167309. DOI: 10.1016/j.ijleo.2021.167309.

[34] Nadimi, M., Saravani, A.Z., Aroon, M.A., Pirbazari, A.E. (2019). Photodegradation of methylene blue by a ternary magnetic TiO_2/Fe_3O_4/graphene oxide nanocomposite under visible light. *Materials Chemistry and Physics*, 225, 464–474. DOI: 10.1016/j.matchemphys.2018.11.029.

[35] Wilson, M., Cheng, C.Y.C., Oswald, G., Srivastava, R., Beaumont, S.K., Badyal, J.P.S. (2017). Magnetic recyclable microcomposite silica-steel core with TiO_2 nanocomposite shell photocatalysts for sustainable water purification. *Colloids and Surfaces A: Physicochemical and Engineering Aspects*, 523, 27–37. DOI: 10.1016/j.colsurfa.2017.03.034.

[36] Sun, A.C. (2018). Synthesis of magnetic carbon nanodots for recyclable photocatalytic degradation of organic compounds in visible light. *Advanced Powder Technology*, 29(3), 719–725. DOI: 10.1016/j.apt.2017.12.013.

[37] Su, T.L., Chiou, C.S., Chen, H.W. (2012). Preparation, photocatalytic activity, and recovery of magnetic photocatalyst for decomposition of benzoic acid. *International Journal of Photoenergy*, 2012, 909678. DOI: 10.1155/2012/909678.

[38] Handoko, E., Budi, E., Sugihartono, I., Marpaung, M.A., Jalil, Z., Taufiq, A., Alaydrus, M. (2020). Microwave absorption performance of barium hexaferrite multinanolayers. *Materials Express*, 10(8), 1328-1336. DOI: 10.1166/mex.2020.1811.

Copyright © 2023, ISSN 1978-2993